Investigation of CO2 storage in a saline formation with an angular unconformity at the caprock interface

Shariatipour, SM, Pickup, GE & MacKay, EJ

Original citation & hyperlink:
Shariatipour, SM, Pickup, GE & MacKay, EJ 2016, 'Investigation of CO2 storage in a saline formation with an angular unconformity at the caprock interface' *Petroleum Geoscience*, vol 22, no. 2, pp. 203-210
https://dx.doi.org/10.1144/petgeo2015-039

DOI 10.1144/petgeo2015-039
ISSN 1354-0793
ESSN 2041-496X

Publisher: Geological Society

Investigation of CO_2 Storage in a Saline Formation with an Angular Unconformity at the Caprock Interface

Seyed M Shariatipour[1*], Gillian E Pickup[2] and Eric J Mackay[2]

[1]Flow Measurement and Fluid Mechanics Research Centre, Coventry University, Priory Street, Coventry CV1 5FB, UK

[2]Heriot-Watt University, Riccarton, Edinburgh EH14 4AS, UK

Corresponding author's email: Seyed.Shariatipour@coventry.ac.uk

Abstract

Studies of oil reservoirs show that unconformities may occur between the reservoir and the caprock. At the boundary where the unconformity occurs, there may be a layer of higher permeability compared to caprock. Such traps may occur at CO_2 storage sites, and therefore their effect should be investigated. In this work, we simulate CO_2 storage beneath angular unconformities, where sandstone layers have been tilted and eroded prior to the deposition of a caprock. After preliminary studies into the effect of gridding such traps, we describe simulations of a range of 2D and 3D models. The results reveal that migration of CO_2 is influenced by the lithology beneath the unconformity which could have been modified by weathering or diagenesis. This can have both positive and negative effects on CO_2 storage capacity and security. It shows that an unconformity model which has a layer of high permeability at the interface between the aquifer and the caprock, as a result of weathering or diagenesis, can contribute to pressure diffusion across the reservoir. This could improve CO_2 sequestration by providing pathways for CO_2 migration to access other parts of the storage complex. On the other hand, this could have a negative effect on the security of CO_2 storage by providing pathways for CO_2 to migrate out of the storage formation and increase the risk of CO_2 leakage.

Keywords

Carbon capture and storage, Angular Unconformity, Interface between Caprock and Storage Formation

Introduction

Carbon Capture and Storage (CCS) is a possible option to significantly mitigate anthropogenic CO_2 emissions to the atmosphere (Bruant et al. 2002; IPCC 2005). Deep saline formations offer the greatest capacity for CO_2 storage (Gunter et al. 1998; Celia et al. 2002; IPCC 2005; SCCS 2009). Such aquifers are widely distributed (Firoozabadi and Cheng 2010) and they are the most promising formations for subsurface storage worldwide (Orr, 2009). The total P50 theoretical storage capacity for the UK continental Self (UKCS) is estimated to be around 60 Gt in saline aquifer formations (Bentham et al. 2014). Many studies of CO_2 storage assume a smooth interface with a sharp transition from aquifer to caprock, whereas typically the surface is irregular, due to the sedimentological setting and structural deformation. For example the CO_2 plume in the Utsira formation at the Sleipner storage site has an irregular outline at the top of the aquifer, as imaged using seismic data (Chadwick and Noy, 2010). The importance of characterisation of the interface between the caprock and the aquifer was investigated by Shariatipour et al. (2012; 2014), Nilsen et al. (2012), Goater et al. (2013) and Newell and Shariatipour (2016). This work follows on from the aforementioned studies, and investigates the effect of unconformable interfaces on the storage capacity and security, an issue which has not been studied previously.

A structural or stratigraphic trap is an important criterion for CO_2 sequestration. Structural and stratigraphical trapping occurs where the migration of free phase CO_2 is prevented by low permeability layers (caprocks) such as layers of mudstone (Chadwick et al. 2008). Usually, there

48 is a major gap in the geological sequence between one rock and overlaying strata, because of
49 non-deposition and/or erosion; this is known as an unconformity (Sloss 1963). Unconformities
50 have been studied extensively, especially because of the types of trap they provide for oil and
51 gas in geological formations. In the North Sea and several other sedimentary basins, a style of
52 trapping is found which results from the truncation of inclined permeable beds by a very low
53 permeable unconformity surface (Archer and Wall 2012). For example, in the Viking Graben area
54 of the northern North Sea, the Brent Sand reservoirs are characteristically faulted deltaic sands
55 truncated by the Cretaceous unconformity (Archer and Wall 2012). In Weyburn in Saskatchewan
56 in Canada there is a zone, ranging in thickness from 2 to 10m, immediately underneath the Sub-
57 Mesozoic Unconformity surface, in which the petrophysical properties have been altered as a
58 result of a combination of dolomitisation, micritisation and anhydritisation and this has made a
59 highly effective seal to fluid migration (Whittaker 2004). Unconformity traps are broadly
60 identified as a class of stratigraphic traps, but they may be influenced by diagenetic processes
61 (Rittenhouse 1972; Biddle and Wielchowsky 1994). There are four types of unconformity:
62 angular unconformity, disconformity, paraconformity and non-conformity (Dunbar and Rogers
63 1957). In this work the focus is on angular unconformities. An angular unconformity is caused by
64 erosion of underlying sediments that have been previously folded or tilted.

65 The term “unconformity surface” is used here to describe the following scenarios. Just above
66 the unconformity, or just below it, there may be a high or low permeability layer. The high
67 permeability layer could be the result of weathering and erosion at the top of the older layer, or
68 could be due to the deposition of coarse-grained sediments on top of the unconformity surface
69 (Swierczek, 2012). Swierczek (2012) studied the base Permian Unconformity in the Southern
70 North Sea and describes a theory that a zone just beneath the Permian unconformity had been
71 weathered, and consequently the permeability and the porosity of this zone had increased

dramatically (average porosity changed from 0.1 to 0.2 and average permeability changed from 0.1-10 mD to 500 mD) (Besly et al, 1993). The existence of a high permeability layer at the unconformity surface has also been noted at the other locations around the world. For example, Rogers et al. (2006) studied the Belfast Bay in the western Gulf of Maine and presented evidence that an unconformity surface can act a conduit for gas migration. They believed that the gas migrates along the Pleistocene/Holocene unconformity surface through a coarse-grained layer which is much more permeable than the rest of the mudstone, and varies in thickness from decimeters to two metres. In another work by Cao et al. (2005), lateral fluid migration along an unconformity surface was confirmed through their study of the Permian petroleum system in the northwest margin of the Junggar Basin. Fengjun et al. (2001) studied lateral migration pathways of hydrocarbons in the Pearl River Mouth Basin, South China Sea. They concluded that oil and gas migrates laterally through an unconformity surface where there is high porosity and permeability sandstone deposited. In this work, the effect such a structure has on CO_2 storage is studied.

Outline of the Paper

This paper consists of three sections. In the first section, due to the slope of the layers in an angular unconformity, an investigation on the effect of gridding type on CO_2 storage will be described before outlining the modelling of the unconformity. In the second section, 2D models will be presented and in the third section, 3D modelling will be discussed. A number of 2D and 3D numerical simulations were conducted to study the impact of unconformities on CO_2 storage. All models were constructed in Petrel, and the reservoir models were input to the ECLIPSE reservoir simulator.

Section 1: An investigation on the effect of gridding type on CO_2 Storage

Spatial discretisation is used to perform the numerical block to block flow calculations in fluid flow simulation. In geo-modelling software there are different options to grid the models. During model construction, when dividing the zones into different layers, the layer thicknesses can be proportional to the thickness of the zone, fractional, or follow the top or the base of the zone, allowing for onlap and truncation to be represented as appropriate. When simulating CO_2 storage in an aquifer, the calculated CO_2 migration pathway may depend on the type of gridding used. In this study the effects of different gridding techniques were investigated. Two sets of grids were examined, the first corresponding to a regular 100×1×71 flat grid (Model CG, Figure 1), and the second corresponding to a 50×1×131 tilted grid (corner point geometry) (Model TG, Figure 1). Both models have the same pore volume and each model is divided into three sections. The upper part of the models, which consists of a single layer, corresponds to the caprock. The second part, referred to as the interface between caprock and storage formation, consists of ten layers. Regular Cartesian grid cells are used in these layers in both models. The third part, which is assumed to be the storage aquifer, is different in terms of grid orientation. In Model CG, a regular Cartesian grid was used and the aquifer was discretised into 50 layers in the vertical direction, each layer being 5 m thick. For Model TG, although the thickness of each layer is the same as in Model CG, the numbers of layers (120) is greater, as they dip at an angle of 1.72.

When CO_2 is injected into an aquifer, it migrates upwards due to buoyancy. The upward migration may be delayed due to the presence of low permeability layers (Juanes et al. 2006; Flett et al. 2007). However, the CO_2 will eventually reach a low permeability caprock and then begins to migrate laterally (Emami-Meybodi et al. 2015). In Model TG, at the top of the storage formation where the tilted grid cells meet the regular horizontal grid cells, all of the tilted grid

cells pinch out. The aquifer was assumed to be homogeneous: the aquifer (sand) was assigned a permeability of 1000 mD and a porosity of 0.25, and the other zones (caprock and interface) were assigned a permeability of 1×10^{-6} mD and a porosity of 0.1. An injector was placed on the left hand side of both 2D models. The wells were controlled by the surface injection rate which was 1,000,000 m^3/day with a maximum pressure limit of 200 bars. The injectors were shut in after 50 years and the simulations were continued for 1000 years. Zero-flow boundaries were assumed to be present at all models edges. The same fluid and rock properties were used for both models. The initial pore fluid pressure was assumed to be hydrostatic, around 90 bar at the top of the storage structure.

Results

Figure 2 shows lateral migration of CO_2 at the top of the aquifer in Models CG and TG at different time steps. At the very top of the aquifer in Model CG, CO_2 migrates laterally away from the injector. In Model TG, the CO_2 cannot migrate laterally by moving horizontally from one cell to the next, due to the cells pinching out. CO_2 must move to a stratigraphically lower (deeper) cell before migrating laterally (Figure 2). The difference in CO_2 migration in these models can be observed from Figure 2 where CO_2 migrates further away from the injector at the top of the aquifer in Model CG compared to Model TG. For example, in Model CG at the 11th time step CO_2 reached 600m (the 6th cell) on the right hand side of the injector (left diagram), whereas in Model TG, at the same time step, CO_2 reached 500m (the 5th cell) on the right hand side of the injector (right diagram).

Figure 3 demonstrates the distribution of the CO_2 plume in Models CG and TG at the end of the post injection period. It is clear that the plume migrates further (around 800m) in Model CG than Model TG. However, the thickness of the plume in Model TG is greater than that in Model

CG. This is because of the way that cells are oriented at the top of the aquifer in Model TG; subsequently there is more accumulation of CO_2 at the top of the aquifer. Regarding the amount of CO_2 dissolved in brine, in Model CG (regular Cartesian grids), CO_2 migrates further at the top of the aquifer than Model TG, and so more free phase CO_2 is in contact with the fresh brine resulting in more CO_2 dissolution (10% increase) in Model CG than Model TG (Figure 4). Since there is more dissolution in Model CG, there is less free CO_2 and therefore the average field pressure is lower.

Discussion on the effect of type of gridding on CO_2 Storage

This part of the study compares the effect of different gridding techniques available in the reservoir simulator for the simulation of CO_2 storage in aquifers. The results reveal that the calculations are sensitive to the gridding choices made. Specifically, where there are some tilted layers it may be necessary to use a tilted grid to represent some of these layers. The current study shows that using a tilted grid for tilted layers in the storage formation leads to a decrease in the distance migrated by the CO_2, both during injection and during the post injection period. This effect is more significant where these inclined grids pinch out such as, in Model TG at the top of the aquifer.

The results demonstrate that the way in which the model is gridded affects the CO_2 migration distance and the amount of dissolution. The main reason is due to the inclined cells pinching out at the top of the storage formation in the tilted grid model. In this model CO_2 must move to a lower (deeper) cell before migrating laterally and therefore it migrates a shorter distance from the injector than in the regular Cartesian grid model. This fact does not affect our modelling results in the next section, because all the models will be constructed in the same manner. Regular flat Cartesian grid will be used for the 2D models and corner point geometry will be

165 used for the 3D models and then the results of equivalently gridded systems are compared.

166 **Section 2: 2D Models**

167 This is an analysis of the effect of a thin conductive layer (as a result of weathering at the
168 unconformity surface) at the aquifer-caprock interface. The rationale for conducting this
169 modelling is based on the results of research by Swierczek (2012) on the role of unconformities
170 in controlling reservoir properties. A 2D model with a length of 10 km, thickness of 400 m, and a
171 width of 100 m was used (Figure 5). This model was devised to investigate migration out of
172 Aquifer 1, which was assumed to be the storage formation. Seven Models were considered
173 (Table 1). The only difference between Model 1, Model 2, and Model 3 being the thickness of
174 the high permeability layer beneath the caprock. The thickness of the high permeability layer in
175 Model 1, Model 2, and Model 3 was 100 cm, 10 cm, and 1 cm respectively. The aquifers were
176 assumed to be homogeneous. The aquifers and the thin layer below the caprock were assigned
177 a permeability of 1000 mD and a porosity of 0.25, and the other reservoir lithologies were
178 assigned a permeability of 1×10^{-6} mD and a porosity of 0.1. To investigate the effect of grid
179 refinement, Model 1 was modified to Model 4 by refining the highly permeable layer below the
180 caprock from one layer to ten layers. Model 5 is based on Model 4, but the perforations in the
181 injector well were at the lower part of Aquifer 2 while the location of the injector was the same
182 as in Model 4. Models 6 and 7 are the same as Models 4 and 5, respectively, apart from the
183 properties of the layer below the caprock. In these cases, the high permeability layer was
184 replaced with low permeability rock, equal to the permeability of the caprock, and the interface
185 region (R2) was assumed to be part of R1 (See Figure 5). To aid in the description of the results,
186 the models were divided into seven regions (Table 2 and Figure 5).

187 A single injector was placed on the left hand side of model and CO_2 injected through

perforations at the bottom of Aquifer 1 (R4) was simulated. The well was controlled by surface rate (20,000 m^3/day) with a maximum pressure limit of 229 bars. However, in all models studied here the same volume of CO_2 was injected, since as the pressure did not reach the limiting bottom-hole pressure. The injector was shut in after 50 years and the simulation was continued for 200 years.

Results and Discussions for 2D Models

In Models 1–3, CO_2 injected into Aquifer 1 is able to migrate to Aquifer 2 via the high permeability layer at the interface between storage formation and caprock. In Model 1 (which had the thickest high permeability layer) the free phase CO_2 migrates more easily through the high permeability layer than in Model 3; consequently there is more CO_2 dissolved in Aquifer 2 in Model 1 than in Model 3 (Figure 6 and Figure 7). However, more CO_2 is dissolved in Model 3 overall due to the greater pressure increase compared to Model 1 in Aquifer 1. Figure 8 illustrates the pressure increase in Models 1, 2, and 3 (all models had the same initial reference pressure constraint). In Model 1, the case with the thickest high-permeability layer beneath the cap rock, this high-permeability layer strongly contributes to the pressure diffusion from Aquifer 1 to Aquifer 2 at the end of the injection period. However, in Model 3 this is not the case because it has the thinnest high permeability layer (Figure 8). Interestingly, 200 years after the well is shut in, the average pressure in Aquifer 2 in Model 1 exceeded the average pressure in Aquifer 1 whereas in Model 3 the average pressure in Aquifer 1 did not change significantly from the average pressure at the end of injection. Figure 9 compares the average pressure in each region in Models 1 and 3. The average pressures in the low permeability layers are the same both at the end of the injection period and the post injection period. However, the pressure in the high permeability unconformity interfaces (Region 2) increases due to the gas migration

211 through them (Figure 9). In Model 3 the average pressure in Aquifer 2 (R6) is lower than Aquifer
212 1 (R4) even 200 years after well shut in due to lower CO_2 migration into it.

213 In Model 3, compared to Model 1, more CO_2 is dissolved in brine in Aquifer 1 (R4) because the
214 pressure is increased (e.g. Spycher and Pruess, 2005). However, more CO_2 is dissolved in Aquifer
215 2 (R6) in Model 1 than Model 3 (Figure 10) due to greater CO_2 migration through the 1 m thick
216 permeability layer into that aquifer. Model 4 is a refined version of Model 1, and in this case,
217 there is slightly more free CO_2 at the end of the post injection period than Model 1 (Figure 11)
218 due to better resolution of the CO_2 plume in the refined region in Model 4. Figure 12 compares
219 the amount of CO_2 dissolution in Models 4-7. Firstly, comparing Models 4 and 5, and 6 and 7,
220 more dissolution of CO_2 takes place when the well is perforated in Aquifer 2. This is because the
221 CO_2 migration path is greater in Aquifer 2, which encourages more dissolution. Comparing
222 Models 4 and 6, and 5 and 7, there is more dissolution when there is no high permeability layer
223 at the unconformity. This means that the CO_2 is confined to a single aquifer, so the pressure
224 increases, giving rise to more dissolution.

225 **Section 3: 3D Models**

226 Here a single 3D Model for an angular unconformity is presented (Figure 13). This figure shows a
227 set of dipping layers which lie beneath the unconformity (shown by the dashed line) prior to the
228 deposition of shale (cap rock). The model has dimensions of 5000 m × 10000 m × 400 m. The
229 properties for the model were taken from Smith et al. (2012) (Lincolnshire model) and are listed
230 in Table 3. Sequential Gaussian simulation was used to generate the porosity and permeability
231 distribution. The correlation length was 1 km in the horizontal direction and 10 m in the vertical
232 direction. The Model was discretised into 25×50×131 cells. Ten vertical wells were placed across
233 the X direction on the left side of the Model. ECLIPSE 300 with the CO2STORE module was used

for all the simulations which were carried out for a period of 250 years. Three components (CO_2, Water and Salt) were considered. The models initially consisted of 100% brine, and 100% supercritical CO_2 was injected during the injection period. All injectors were shut after 50 years and simulations were continued for 200 years. The same volume of CO_2 was injected in all models. Both storage formations, aquifer 1 and aquifer 2 (Figure 13), contact the left side of the model. Therefore this side of the model was assumed open, and a porosity multiplier of 1000 was applied to the left hand column to represent additional aquifer pore volume.

To study the effect of the unconformity surface on CO_2 storage in this 3D Model, four models (A, B, C and D) were defined by changing the properties of the 1 m thick layer just above the unconformity surface (Table 4). The permeabilities and porosities of that layer were varied from high values (Sandstone) to low values (Mudstone) to investigate the CO_2 migration beneath the caprock. Model A, could be the result of material with high permeability being deposited. Model B (patchy interface), could be the result of material with low permeability also being deposited. In Model C there is no difference between the properties of this layer and the layers above it; in other words, this layer has the same properties as the caprock.

Results and Discussion for 3D Models

Figure 14, Figure 15 and Figure 16 show the CO_2 gas saturation in brine for models A, B and C respectively, at the end of the injection period (50 years) and 200 years post injection. They illustrate how the unconformity surface affects the CO_2 migration beneath the cap rock. After CO_2 is injected into Aquifer 1 (Primary storage) near the lowest point of the aquifer, it migrates up dip due to buoyancy, until it reaches the caprock. Then, depending on the nature of the layer above the unconformity surface between the caprock and the storage formation, CO_2 migrates laterally. If the unconformity surface has high permeability (e.g. Model A) the plume can easily

migrate in all directions, away from injectors, beneath the caprock (Figure 14). There are advantages and disadvantages associated with this. Regarding the advantages, CO_2 migrates laterally until it reaches another high permeability formation (e.g. aquifer 2 in this model). Therefore more CO_2 is in contact with brine, so more CO_2 dissolves, thus increasing storage capacity and security. On the other hand, CO_2 escapes from the primary storage and therefore the structural trapping is not very effective. Model B is similar to Model A, but with a more irregular CO_2 distribution (Figure 15). Model C demonstrates the importance of the layers underlying an aquifer when there is an unconformity. In Model C the properties of both layers below and above the primary storage are the same as the cap rock properties, and it acts as a seal; thus, it does not allow CO_2 to migrate to Aquifer 2 (Figure 16).

Sensitivity Analysis: Sensitivity to Thickness of Highly Permeable Layer above the Unconformity

The thickness of the layer above the unconformity surface was initially 1 m, in Model A. In Model D it is increased to 10 m. In Model A there is a 1 m highly permeable layer whereas in Model D there is a 10 m highly permeable layer just above the unconformity surface. Figure 17 compares the mole fraction of CO_2 dissolved in brine in these two Models after the 50 years injection period (left images) and after 200 years post injection (right images). The results show that the thinner the highly permeable layer, the slower the lateral CO_2 migration; hence more CO_2 is dissolved near the injectors. During the post injection period, CO_2 migrates slower in Model A than Model D. In Model D, the CO_2 begins to fill Aquifer 2 once it has reached the top of this aquifer. This downward migration is controlled by the height of the CO_2 column on the primary storage (on the left side of the model), as there is a closed boundary condition on the right hand side of model.

Concluding remarks

The positive and negative roles of an unconformity surface as an interface between caprock and storage formation on the CO_2 sequestration has been studied in this paper. Firstly, the effect of gridding type on CO_2 storage was investigated due to the dip of layers in an angular unconformity model. This effect is more significant where these inclined cells pinch out. The findings of this study are very important in modelling of CO_2 storage as they show that selecting different types of gridding leads to an overestimate or an underestimate of the distance migrated by CO_2 and the amount of dissolved CO_2 in the aquifer. Secondly, the results show that an unconformity model which has a layer of high permeability at the interface between the aquifer and the caprock, as a result of weathering, can contribute to pressure diffusion across the reservoir. This could improve CO_2 sequestration by providing pathways for CO_2 migration to access other storage formations (provided CO_2 does not migrate out of the storage complex). Therefore, with appropriate placement of the well in a case where there are stacked dipping aquifers, it is possible to maximize CO_2 storage. The nature of the unconformity may not be known, because it would not normally be detected on seismic, and even if an anomalous permeability value is detected in a well log, the lateral extent may not be known. Therefore, engineers will be unaware whether or not the CO_2 would migrate from one formation to another. In the absence of a high permeability layer either above or below an unconformity, lateral migration of CO_2 is limited. Pressure builds up, but the amount of dissolution increases. In addition, the existence of a high permeability layer at the unconformity surface could have a negative effect on the security of CO_2 storage by providing path ways for CO_2 to migrate out of the storage formation and increase the risk of CO_2 leakage.

Acknowledgements

303 The authors would like to thank the reviewers for useful comments. Authors thank
304 Schlumberger for the use of Eclipse 300 and Petrel and Amarile for the use of the Re-Studio. The
305 project was financed by Scottish Carbon Capture and Storage (SCCS) Consortium and Foundation
306 CMG, which are gratefully acknowledged. We also thank Helen Lever for advice on
307 unconformities.

308
309
310
311
312
313
314
315
316
317
318
319
320
321
322
323
324
325

326 **References**

Archer, J. S., Wall, C. G., 2012. Petroleum engineering: principles and practice. Springer Science & Business Media.

Bentham M., Mallows T., Lowndes J., Green A. 2014. CO_2 Storage Evaluation Database (CO_2 Stored), the UK's online storage database, Energy Procedia 63, 5103-5113.

Besly, B. M., Burley, S. D. & Turner, P. 1993. The late carboniferous barren red bed play of the southern North Sea. Proceeding of the 4th conference. Geological Society, London, Vol. 4, 727-740.

Biddle, K. T., & Wielchowsky, C. C. 1994. Hydrocarbon traps. *Memoirs-American Association Of Petroleum Geologists*, 219-219.

Bruant, R., Guswa, A., Celia, M., & Peters, C. 2002. Safe Storage of CO_2 in Deep Saline Aquifers. Environmental Science and Technology Washington, 36(11), 240A-245A.

Cao, J., Zhang, Y., Hu, W., Yao, S., Wang, X., Zhang, Y., & Tang, Y. 2005. The Permian hybrid petroleum system in the northwest margin of the Junggar Basin, northwest China. *Marine and Petroleum Geology*, *22*(3), 331-349.

Celia, M. A., Peters, C. A., & Bachu, S. 2002. Geologic Storage of CO2: Leakage Pathways and Environmental Risks. In *AGU Spring Meeting Abstracts* (Vol. 1, p. 03).

Chadwick, A., Arts, R., Bernstone, C., May, F., Thibeau, S., & Zweigel, P. 2008. Best practice for the storage of CO_2 in saline aquifers. *British Geological Survey Occasional Publication*, *14*, 267.

Chadwick, R. A., & Noy, D. J., 2010. History-matching flow simulations and time-lapse seismic data from the Sleipner CO_2 plume. In Geological Society, London, Petroleum Geology Conference series (Vol. 7, pp. 1171-1182). Geological Society of London.

Dunbar, C.O. and Rogers, J. 1957. Principles of Stratigraphy, Wiley, New York.

Emami-Meybodi, H., Hassanzadeh, H., Green, C. P., & Ennis-King, J. 2015. Convective dissolution of CO_2 in saline aquifers: Progress in modeling and experiments. *International Journal of Greenhouse Gas Control.*

Fengjun, N., Sitian, L., Hua, W., Xinong, X., Keqiang, W., & Meizhu, J. (2001). Lateral migration pathways of petroleum in the Zhu III subbasin, Pearl River Mouth basin, South China Sea. *Marine and petroleum geology*, *18*(5), 561-575.

Firoozabadi, A., Cheng, P., 2010. Prospects for subsurface CO_2 sequestration. AlChE J. 56 (6), 1398–1405.

Flett, M., Gurton, R., & Weir, G. 2007. Heterogeneous saline formations for carbon dioxide disposal: Impact of varying heterogeneity on containment and trapping. *Journal of Petroleum Science and Engineering*, *57*(1), 106-118.

IPCC. 2005. Intergovernmental Panel on Climate Change, Special Report, Carbon Dioxide Capture and Storage, Summary for Policymakers, Montreal, Canada.

Juanes, R., Spiteri, E. J., Orr, F. M., & Blunt, M. J. 2006. Impact of relative permeability hysteresis on geological CO_2 storage. *Water Resources Research*, *42*(12).

Goater, A., Bijeljic, B. & Blunt, M. J. 2013. Dipping open aquifers—The effect of top-surface topography and heterogeneity on CO_2 storage efficiency. International Journal of Greenhouse Gas Control, 17, 318-331.

Gunter WD, Wong S, Cheel DB, Sjostrom G. Large CO_2 sinks: Their role in the mitigation of greenhouse gases from an international, national (Canadian) and provincial (Alberta) perspective. Appl Energy 1998;61:209–27

Newell, A. J., & Shariatipour, S. M. 2016. Linking outcrop analogue with flow simulation to reduce uncertainty in sub-surface carbon capture and storage: an example from the Sherwood Sandstone Group of the Wessex Basin, UK. *Geological Society, London, Special Publications*, *436*, SP436-2.http://doi.org/10.1144/SP436.2.

Nilsen, H. M., Syversveen, A. R., Lie, K.-A., Tveranger, J. & Nordbotten, J. M. 2012. Impact of top-surface morphology on CO_2 storage capacity. International Journal of Greenhouse Gas Control, 11, 221-235.

Orr Jr., F.M., 2009. Onshore geologic storage of CO_2. Science 325 (5948), 1656–1658.

Ritenhouse, G., 1972. Stratigraphic-Trap Classification: Geologic Exploration Methods, Book Title: Stratigraphic Oil and Gas Fields--Classification, Exploration Methods, and Case Histories, Pub. Id: A010, 14-28.

Rogers, J. N., Kelley, J. T., Belknap, D. F., Gontz, A., & Barnhardt, W. A. 2006. Shallow-water pockmark formation in temperate estuaries: a consideration of origins in the western gulf of Maine with special focus on Belfast Bay. *Marine Geology*, *225*(1), 45-62.

SCCS 2009. Opportunities for CO_2 Storage around Scotland — an integrated strategic research study, 56 pp., Available at: http://www.gov.scot/Resource/Doc/270737/0080597.pdf.

Sloss, L. L. 1963. Sequences in the cratonic interior of North America.Geological Society of America Bulletin, 74(2), 93-114.

Smith, M., Campbell, D, Mackay, E.J. & Polson, D. 2012. CO_2 Aquifer Storage Site Evaluation and Monitoring. SCCS. ISBN: 978-0-9571031-0-8.

Shariatipour, S.M., Pickup, G.E., Mackay, E.J. & Stow, D.A.V. 2012. The Effects of Aquifer/Caprock Interface on CO_2 Storage Capacity and Security. 3rd EAGE CO_2 Geological Storage Workshop, Edinburgh, 25-26 March.

Shariatipour, S. M., Pickup, G. E., & Mackay, E. J. 2014. The Effect of Aquifer/Caprock Interface on Geological Storage of CO_2. Energy Procedia, 63, 5544-5555.

Spycher N.F. & Pruess, K. (2005) CO2–H2O mixtures in the geological sequestration of CO2. II. Partitioning in chloride brines at 12–100 °C and up to 600 bars, Geochim. Cosmochim. Acta 69 (13), pp. 3309–3320.

Swierczek, M. 2012. Role of unconformities in controlling clastic reservoir properties Insights from adopting a multidisciplinary approach, PhD Thesis, Heriot-Watt University, Institute of Petroleum Engineering. Edinburgh.

Whittaker, S. G., 2004. Investigating geological storage of greenhouse gases in southeastern Saskatchewan: The IEA Weyburn CO_2 Monitoring and Storage Project. *Summary of investigations*, *1*, 2004-4.

Figure captions

Figure 1: Regular flat Cartesian grid (Model CG,Top picture) and Tilted grid (Model TG, Bottom Picture).

Figure 2: Gas saturation at the top of the aquifer at 11^{th} time step in Models CG and TG.

Model CG, top picture (Cartesian grid) and Model TG, bottom picture (Tilted grid).

Figure 3 CO_2 Gas saturation at the end of post injection period (White arrow shows length of plume).

Figure 4 CO_2 dissolved in Water Phase in Both Models.

Figure 5 Angular Unconformity 2D Model. R stands for Region.

R2 refers to the unconformity surface and R7 consists of bottom three layers.

Figure 6 Mole fraction of CO_2 dissolved in brine at the end of injection period (50 years) Models 1 and 3.

Figure 7 Mole fraction of CO_2 dissolved in brine 200 Years after well shut in Models 1 and 3.

Figure 8 Pressure increase in Models 1, 2, and 3.

Figure 9 Average pressure in regions 1 to 7 at the end of injection period (left) and 200 years post-injection (right).

Figure 10 The amount of CO_2 dissolved in Models 1 and 3 at the end of injection period (left) and 200 years post-injection (right).

Figure 11 Average free CO_2 Saturation in Models 1 and 4 at the end of injection period (left) and 200 years post-injection (right).

Figure 12 Total amount of CO_2 dissolved in Models 4, 5, 6, and 7.

Figure 13 3D Angular Unconformity Model, illustrating a group of tilted layers that lie beneath the unconformity (red line) prior to the deposition of shale (cap rock).

Figure 14 Top picture shows CO_2 gas saturation in the Model A at the end of injection period (50 years), bottom picture illustrates CO_2 gas saturation in the Model A after 200 years post injection.

Figure 15 Top picture shows CO_2 gas saturation in the Model B at the end of injection period (50 years), bottom picture illustrates CO_2 gas saturation in the Model B after 200 years post injection.

Figure 16 Top picture shows CO_2 gas saturation in the Model C at the end of injection period (50 years), bottom picture illustrates CO_2 gas saturation in the Model C after 200 years post injection.

Figure 17 Model A with a 1m thick high permeability unconformity zone. Model D has a 10-m thick high permeability layer. Left pictures show mole fraction at the end of injection period (50 years) and the right pictures show the CO_2 mole fraction at the end of post injection period (200 years).

Table 1. 2D model details, HP refers to the case where there is a high permeability layer at the interface between storage formation and caprock; LP refers to a low permeability layer at the interface between storage formation and caprock.

Model	Thickness of conductive layer (m)	Number of layers (Refinement)	Primary storage target	Perforations	Permeability
1	1	1	Aquifer 1	bottom four layers of Aquifer 1	HP
2	0.1	1	Aquifer 1	bottom four layers of Aquifer 1	HP
3	0.01	1	Aquifer 1	bottom four layers of Aquifer 1	HP
4	1	10	Aquifer 1	bottom four layers of Aquifer 1	HP
5	1	10	Aquifer 2	bottom four layers of Aquifer 2	HP
6	1	10	Aquifer 1	bottom four layers of Aquifer 1	LP
7	1	10	Aquifer 2	bottom four layers of Aquifer 2	LP

Table 2. Regions in the 2D models

Region	Description
Region 1	Caprock
Region 2	Unconformity interface

Region 3	Low permeable layer above Aquifer 1
Region 4	Aquifer 1
Region 5	Low permeable layer between Aquifer 1 and Aquifer 2
Region 6	Aquifer 2
Region 7	Low permeable layer below Aquifer 2

478

479 Table 3. 3D Model properties.

Formation	**Geometric Average Permeability (mD)**	**Standard Deviation ln(Perm)**	**Average Porosity**	**Standard Deviation Porosity**	**Porosity**	
					Minimum	**Maximum**
Sandstone (Aquifer)	500	0.5	0.2	0.02	0.16	0.25
Mudstone (Cap rock)	0.006	0.1	0.1	0.03	0.06	0.20

480

481 Table 4. 3D model details. "Patchy" refers to the case where there is variable permeability in
482 the layer between the storage formation and the caprock, so there are both high and low
483 permeability cells at the interface. (HP = high permeability, LH = low permeability.)

Model	**Thickness of conductive layer (m)**	**Primary storage target**	**Perforations**	**Permeability**
A	1	Aquifer 1	Aquifer 1	HP
B	1	Aquifer 1	Aquifer 1	Patchy
C	1	Aquifer 1	Aquifer 1	LP
D	10	Aquifer 1	Aquifer 1	HP

484

Figure 1: Regular flat Cartesian grid (Model CG,Top picture) and Tilted grid (Model TG, Bottom Picture).

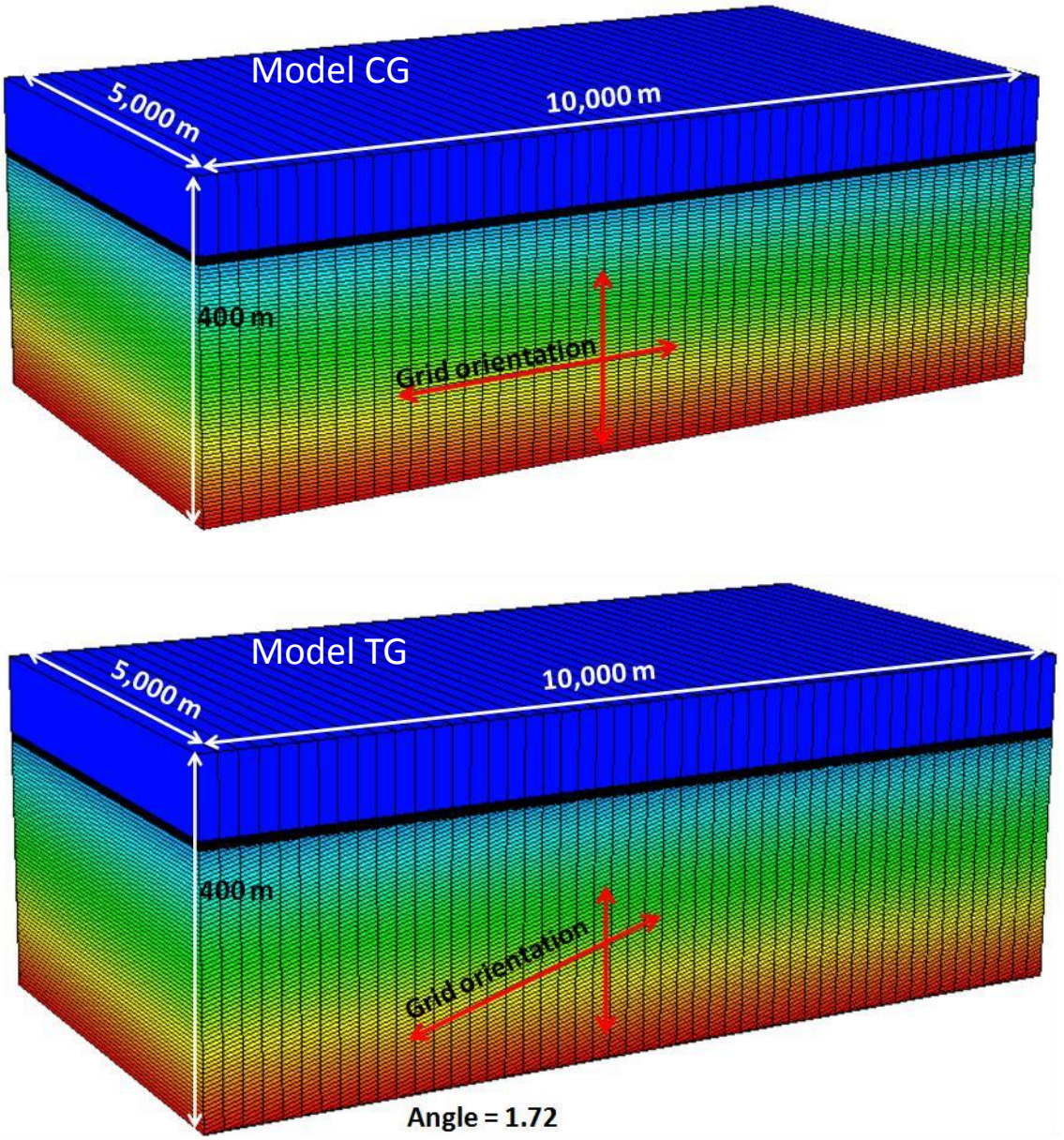

Figure 2: Gas saturation at the top of the aquifer at 11th time step in Models CG and TG. Model CG, top picture (Cartesian grid) and Model TG, bottom picture (Tilted grid).

Figure 3: CO_2 Gas saturation at the end of post injection period (White arrow shows length of plume).

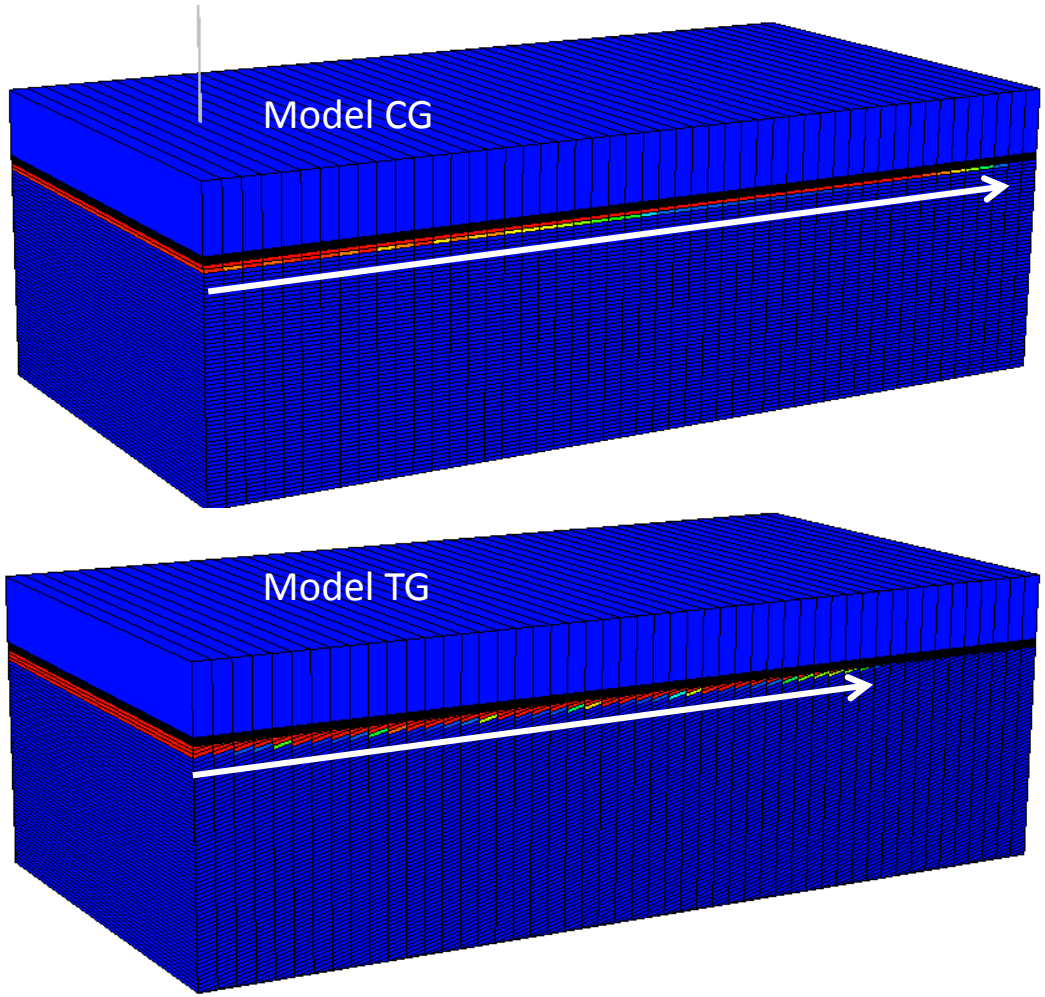

Figure 4: CO_2 dissolved in Water Phase in Both Models.

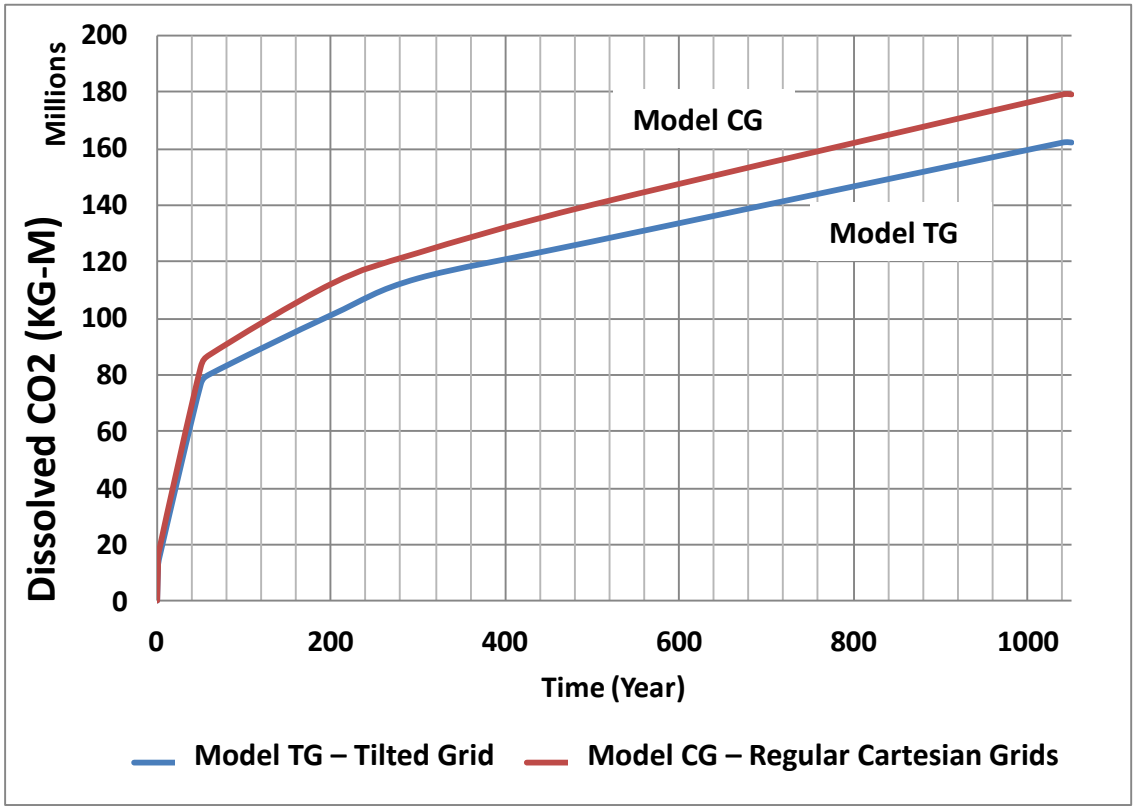

Figure 5: Angular Unconformity 2D Model. R stands for Region.
R2 refers to the unconformity surface and R7 consists of the bottom three layers.

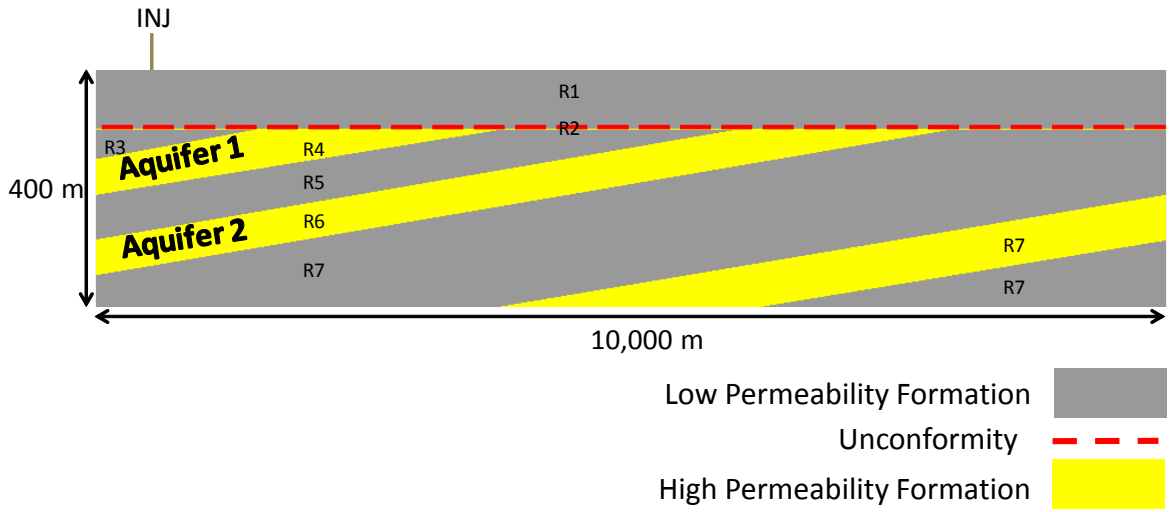

Figure 6: Mole fraction of CO_2 dissolved in brine at the end of injection period (50 years) Models 1 and 3.

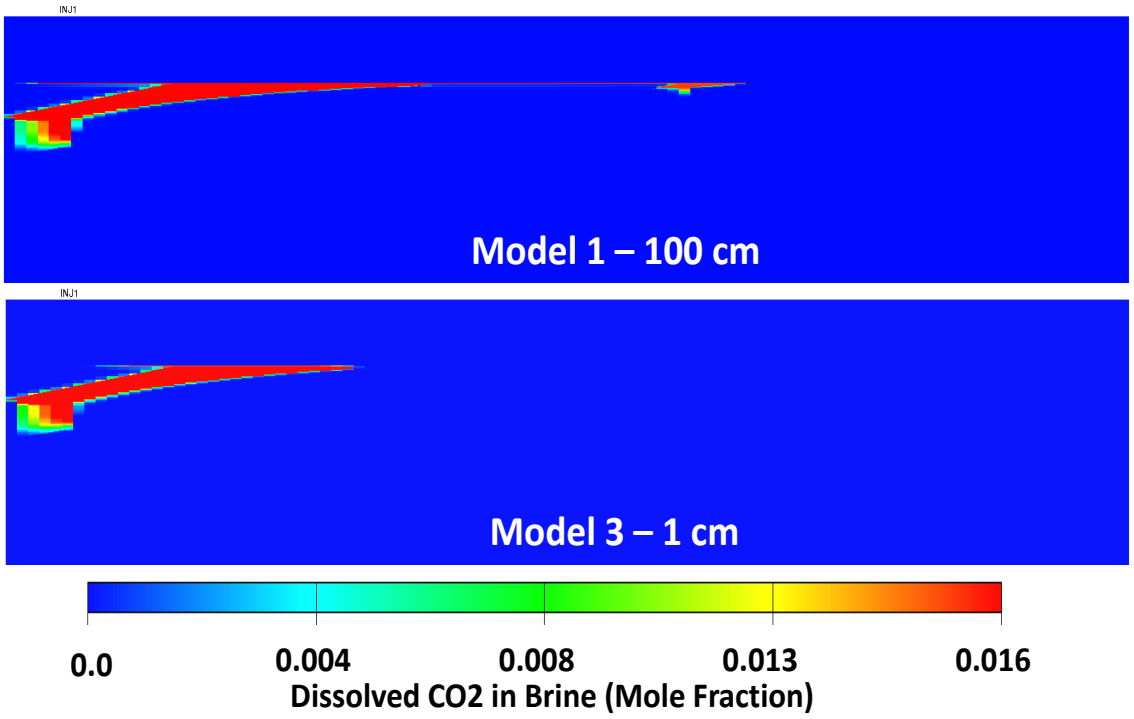

Figure 7: Mole fraction of CO_2 dissolved in brine 200 Years after well shut in Models 1 and 3.

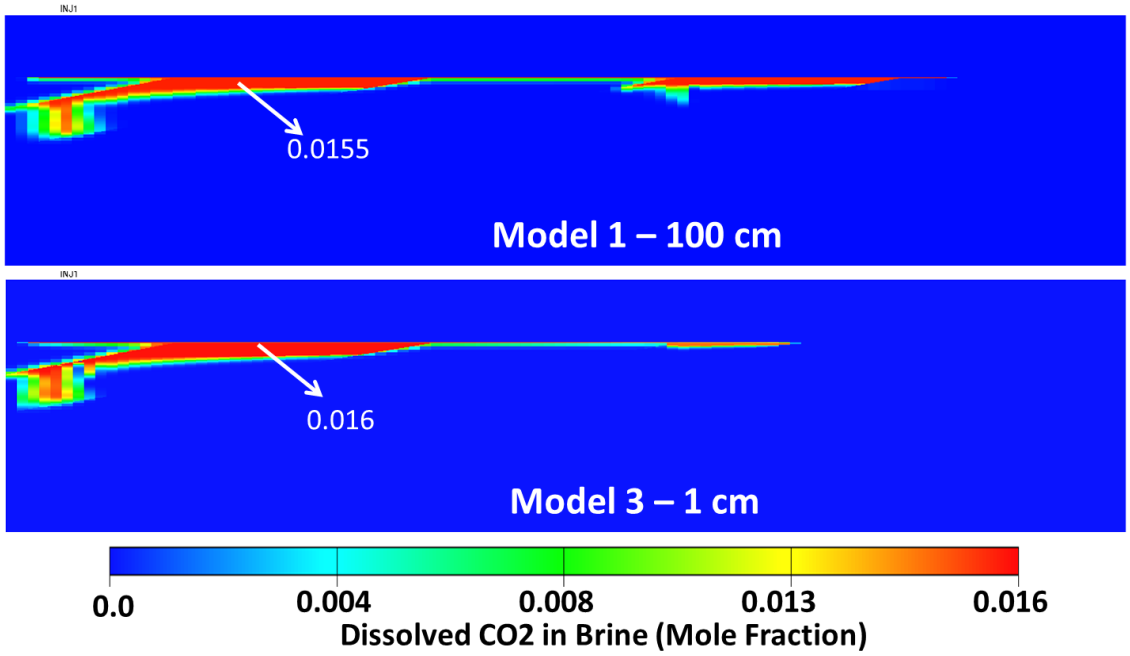

Figure 8: Pressure increase in Models 1, 2, and 3.

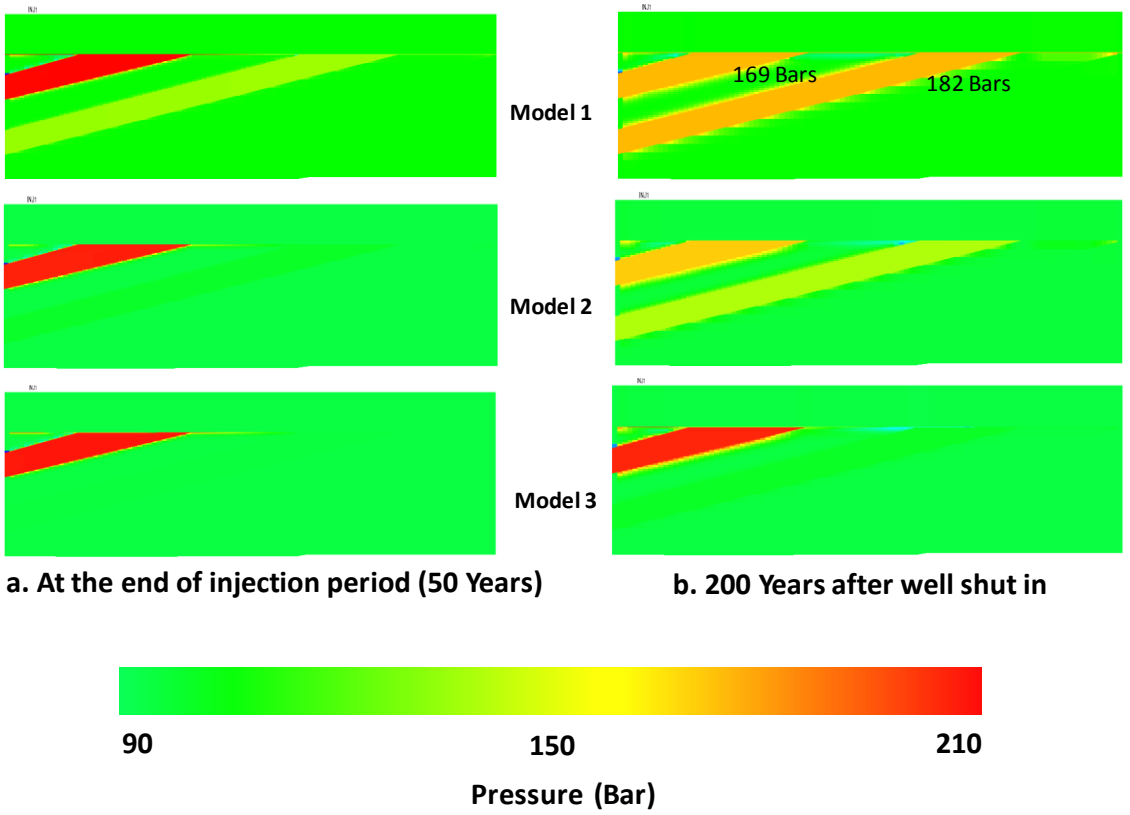

Figure 9: Average pressure in regions 1 to 7
at the end of injection period (left) and 200 years post-injection (right).

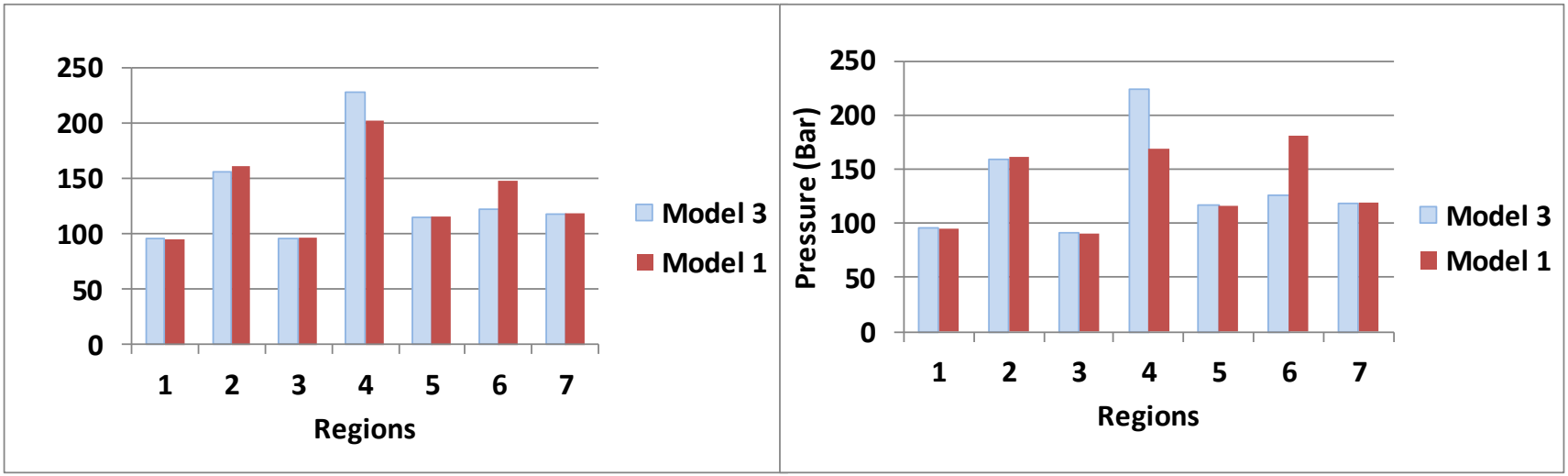

a. At the end of injection period (50 Years)

b. 200 Years after well shut in

Figure 10: The amount of CO_2 dissolved in Models 1 and 3
at the end of injection period (left) and 200 years post-injection (right).

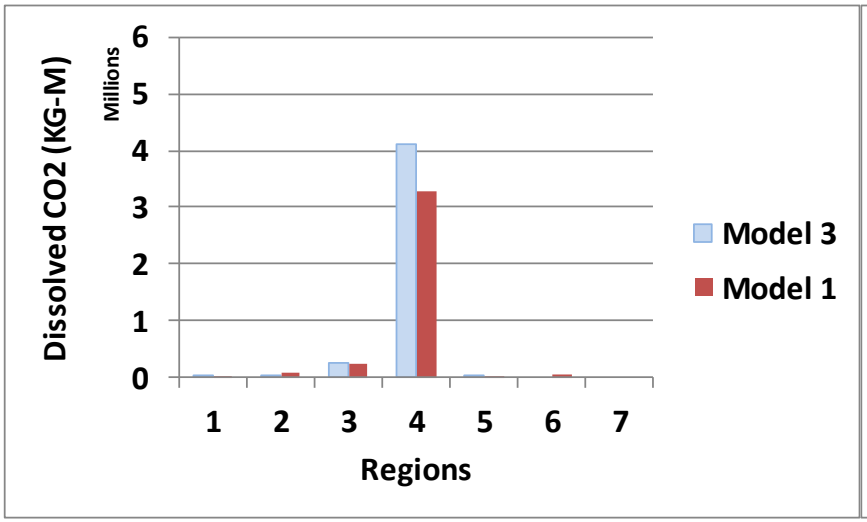

a. At the end of injection period (50 Years)

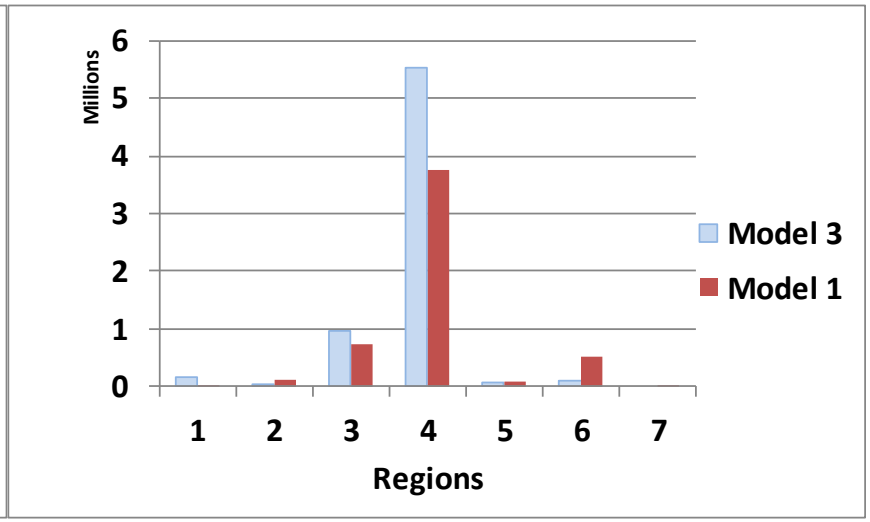

b. 200 Years after well shut in

Figure 11: Average free CO_2 Saturation in Models 1 and 4
at the end of injection period (left) and 200 years post-injection (right).

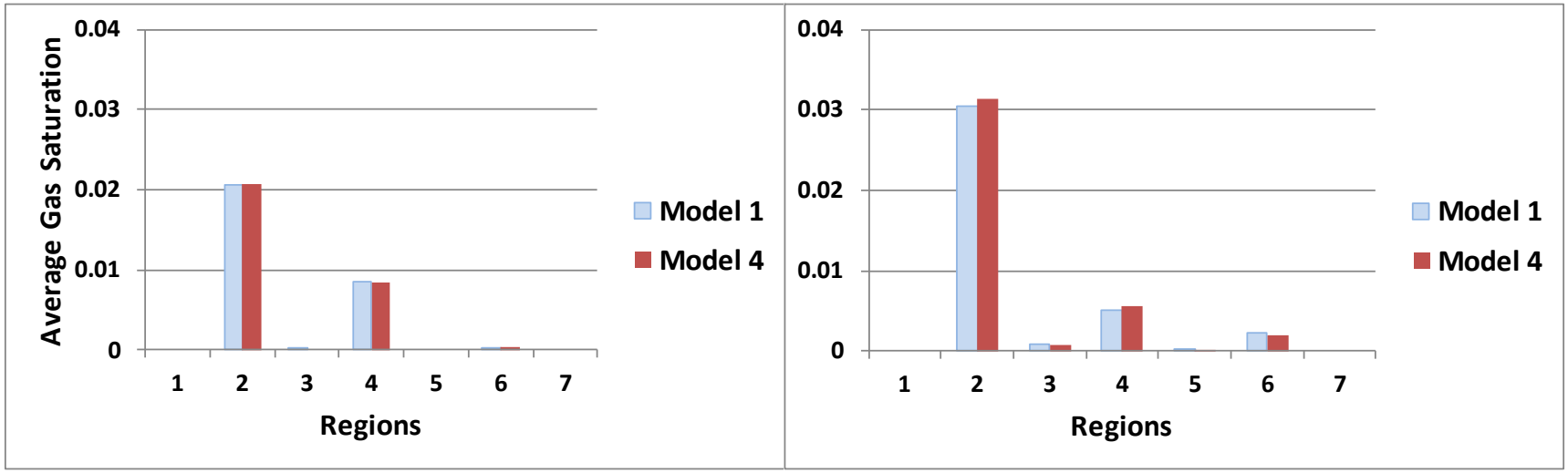

a. At the end of injection period (50 Years)

b. 200 Years after well shut in

Figure 12: Total amount of CO_2 dissolved in Models 4, 5, 6, and 7.

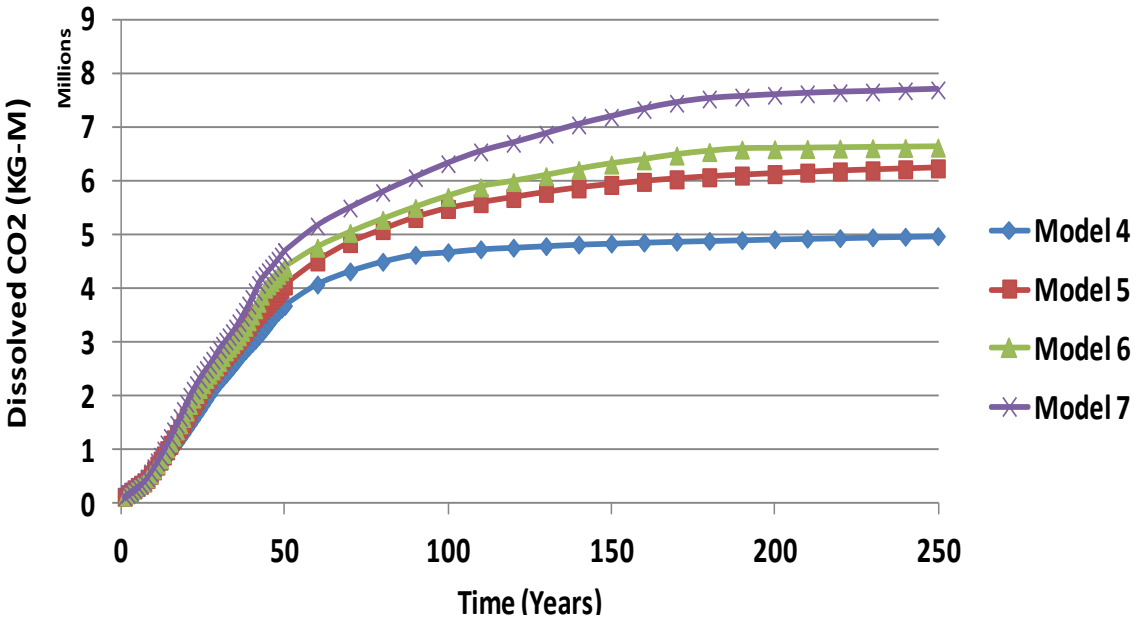

Figure 13: 3D Angular Unconformity Model , illustrating a group of tilted layers that lie beneath the unconformity (red line) prior to the deposition of shale (cap rock).

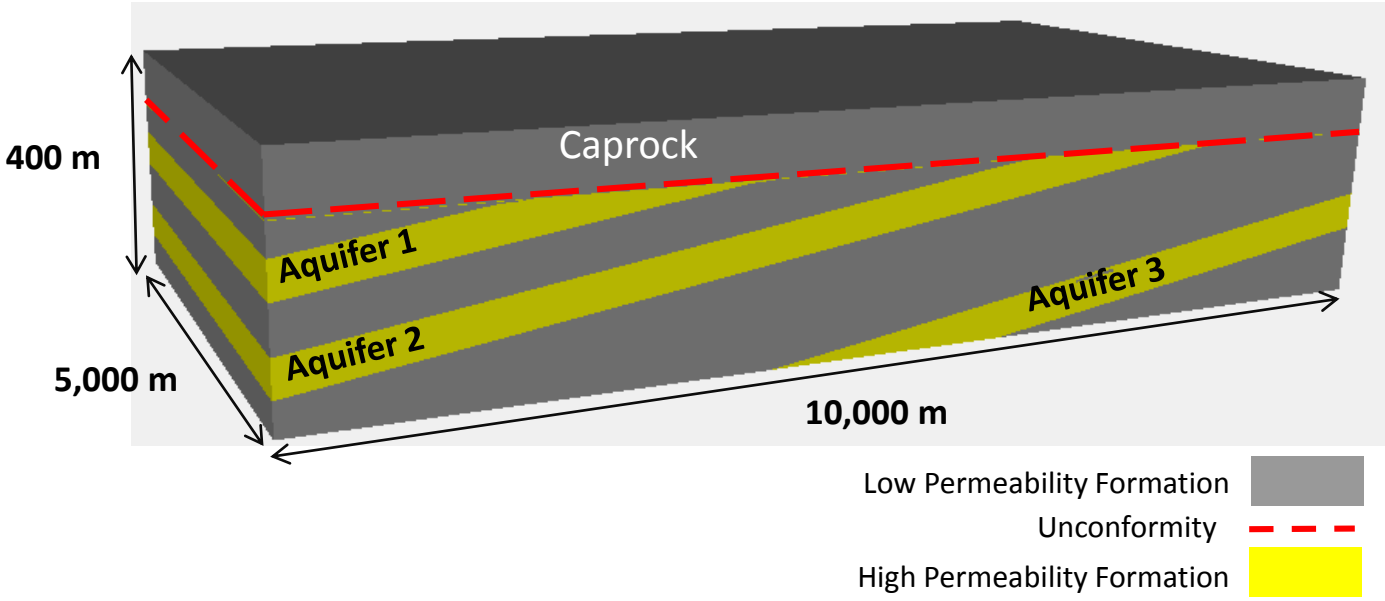

Figure 14: Top picture shows CO_2 gas saturation in the Model A at the end of injection period (50 years). Bottom picture illustrates CO_2 gas saturation in the Model A after 200 years post injection.

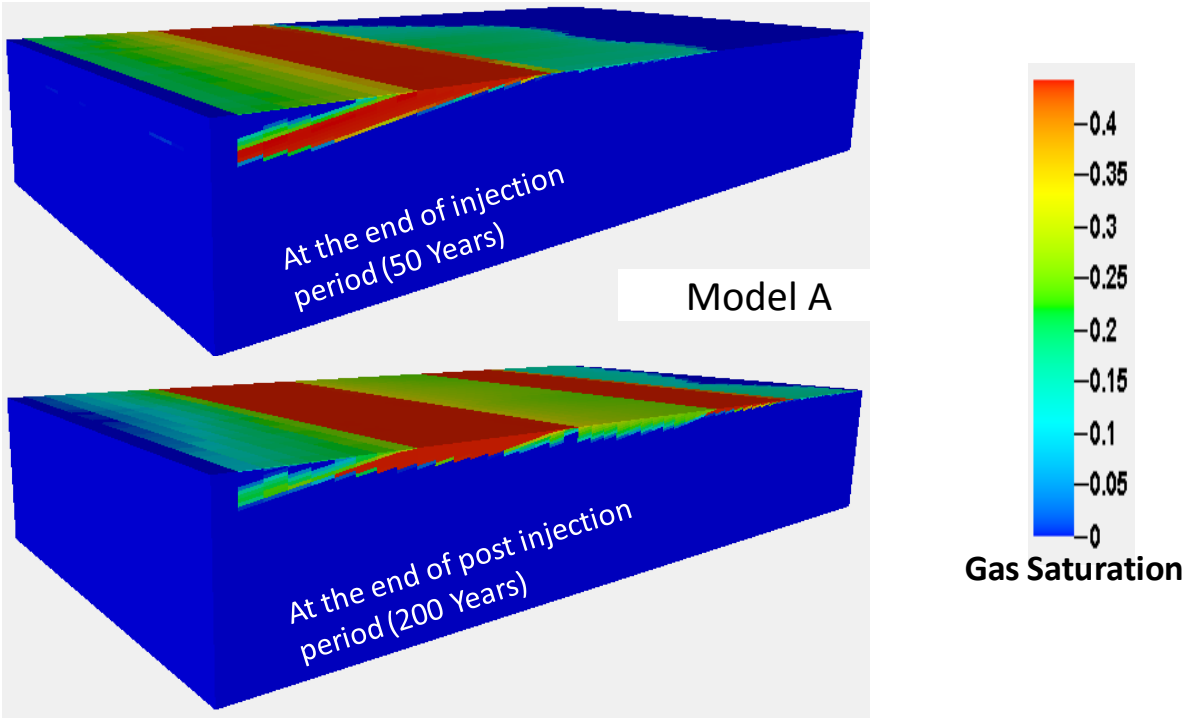

Figure 15: Top picture shows CO_2 gas saturation in the Model B at the end of injection period (50 years). Bottom picture illustrates CO_2 gas saturation in the Model B after 200 years post injection.

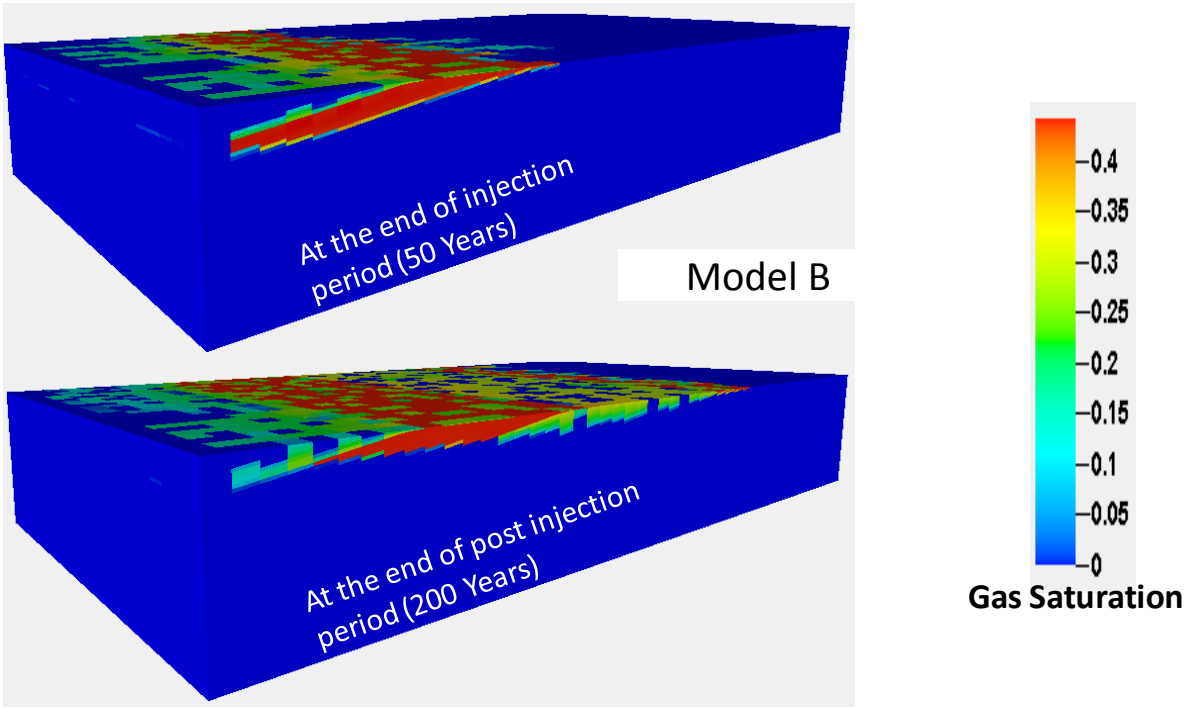

Figure 16: Top picture shows CO2 gas saturation in the Model C at the end of injection period (50 years), bottom picture illustrates CO2 gas saturation in the Model C after 200 years post injection.

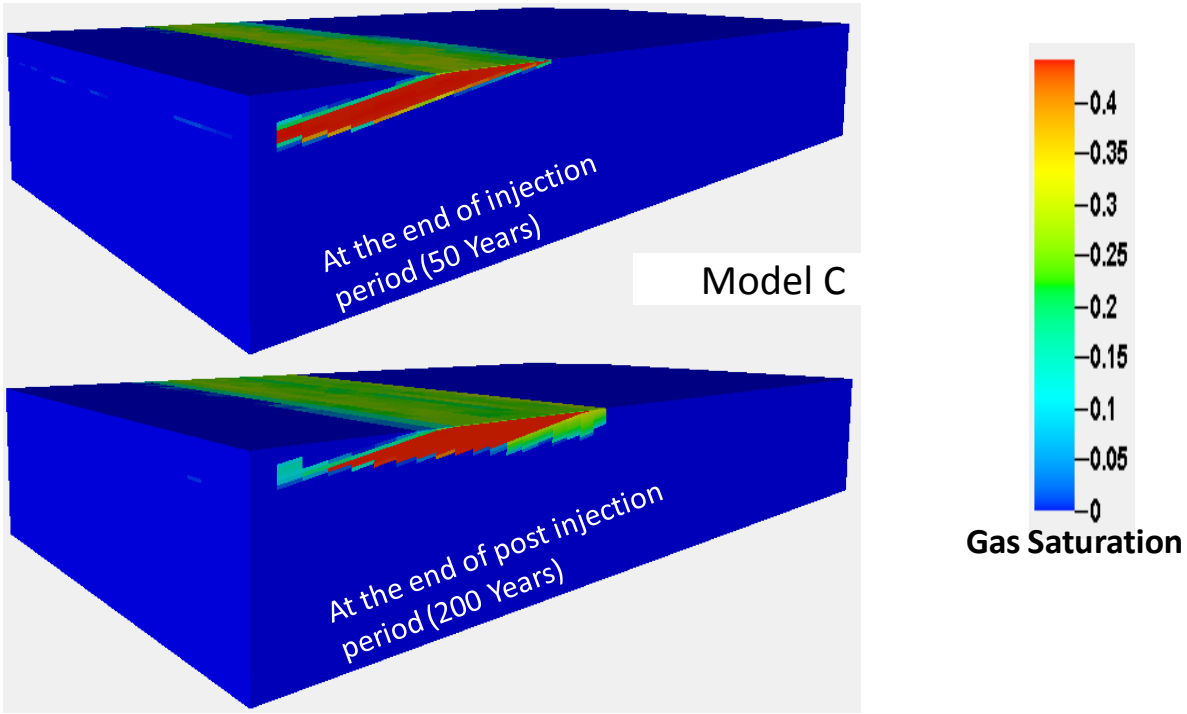

Figure 17: Model A with a 1m thick high permeability unconformity zone. Model D has a 10-m thick high permeability layer. Left pictures show mole fraction at the end of injection period (50 years) and the right pictures show the CO_2 mole fraction at the end of post injection period (200 years).